

GPS++: Reviving the Art of Message Passing for Molecular Property Prediction

Dominic Masters¹ Josef Dean¹ Kerstin Klaser¹ Zhiyi Li¹ Sam Maddrell-Mander¹ Adam Sanders¹
 Hatem Helal¹ Deniz Beker¹ Andrew Fitzgibbon¹ Shenyang Huang^{2,3,4} Ladislav Rampášek^{3,5}
 Dominique Beaini^{2,3,5}

Abstract

We present GPS++, a hybrid Message Passing Neural Network / Graph Transformer model for molecular property prediction. Our model integrates a well-tuned local message passing component and biased global attention with other key ideas from prior literature to achieve state-of-the-art results on large-scale molecular dataset PCQM4Mv2. Through a thorough ablation study we highlight the impact of individual components and, contrary to expectations set by recent trends, find that nearly all of the model’s performance can be maintained without any use of global self-attention. We also show that our approach is significantly more accurate than prior art when 3D positional information is not available.

1. Introduction

Among many scientific areas, deep learning is having a transformative impact on molecular property prediction tasks for biological and chemical applications (Keith et al., 2021; Reiser et al., 2022). In particular, the aim is to replace or augment expensive and/or time-consuming experiments and first-principles methods with more efficient machine learning models. While there is a long history of machine learning methods in this field, two particular approaches have been dominant as of late for processing graph-structured molecular data: message passing neural networks (MPNNs) iteratively build graph representations of molecules by sending information explicitly along edges defined by bonds (Gilmer et al., 2017; Battaglia et al., 2018); while graph transformers treat the nodes (atoms) as all-to-all connected and employ global self-attention approaches (Vaswani et al., 2017), optionally building in local

Table 1. Comparison of ensembled model accuracy on OGB-LSC PCQM4Mv2 dataset with under four-hour inference time constraint. Strong single-model performance and efficient implementation on Graphcore IPU hardware enables a large ensemble to achieve the state-of-the-art accuracy.

Model/Method (Ensemble Size)	Test-Challenge MAE (meV) ↓
Transformer-M, GNN and ResNet (35 models) Darabi et al. (2022)	72.3
Transformer-M-ViSNet and Pretrained-3D-ViSNet (22 models) Wang et al. (2022c)	72.3
GPS++ (112 models)	71.9

inductive biases through augmented attention (Ying et al., 2021a; Luo et al., 2022). While transformers have been extremely successful in other domains, the quadratic complexity with respect to the number of nodes is a significant obstacle for larger molecules. This makes MPNNs an attractive approach due to their linear scaling with graph size, however issues like oversmoothing (Li et al., 2018), oversquashing, and underreaching (Alon & Yahav, 2021) have been found to limit their effectiveness.

In this work we focus on the task of predicting the HOMO-LUMO energy gap, an important quantum chemistry property being the minimum energy needed to excite an electron in the molecular structure. This property is typically calculated using Density Functional Theory (DFT) (Kohn & Sham, 1965), the *de facto* method used for accurately predicting quantum phenomena across a range of molecular systems. Unfortunately, traditional DFT can be extremely computationally expensive, prohibiting the efficient exploration of chemical space (Dobson, 2004), with more than 8 hours per molecule per CPU (Axelrod & Gomez-Bombarelli, 2022). Within this context the motivation for replacing it with fast and accurate machine learning models is clear. While this task does aim to accelerate the development of alternatives to DFT it also serves as a proxy for other molecular property prediction tasks. Therefore it can potentially benefit a range of scientific applications in fields like computational chemistry, material sciences and drug discovery.

¹Graphcore, UK ²Valence Discovery, Canada ³Mila, Canada
⁴McGill University, Canada ⁵Université de Montréal, Canada. Correspondence to: Dominic Masters <dominicm@graphcore.ai>.

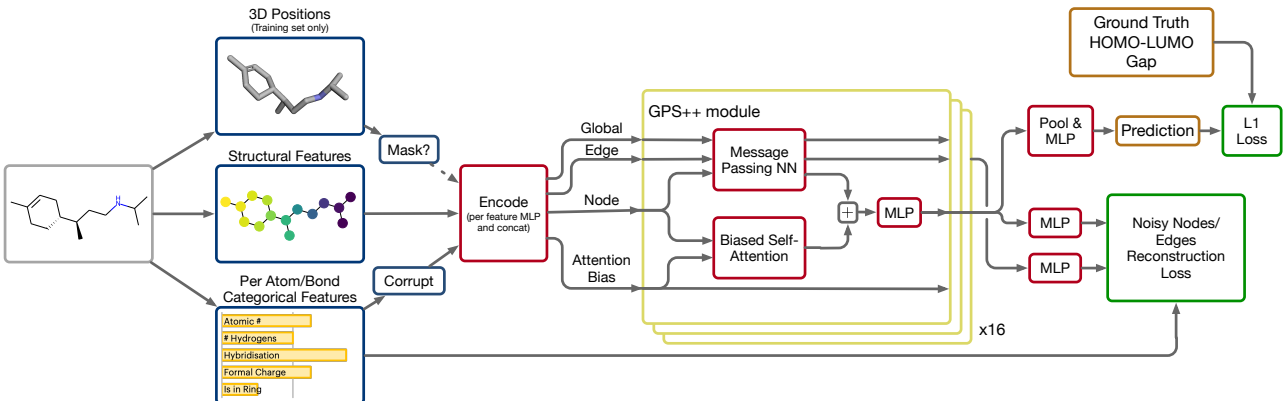


Figure 1. Augmented General Powerful Scalable (GPS++) Graph Transformer overview. (left) GPS++ takes on the input a featurised molecular graph. Chemical, positional, and structural node (atom) and edge (bond) features are detailed in §4.2. Geometric 3D information is provided only optionally during training, e.g. inference on PCQM4Mv2 test set needs to be done without their explicit knowledge. (middle) A stack of GPS++ modules that combine a custom local MPNN and a global biased self-attention mechanism (akin to Transformer-M) to learn expressive representations, see §4.1. (right) Global graph pooling with final prediction head, and auxiliary denoising tasks, see §5.2.

one of the largest widely available DFT databases, and from it is derived the PCQM4Mv2 dataset, released as a part of the Open Graph Benchmark Large Scale Challenge (OGB-LSC) (Hu et al., 2021), which has served as a popular testbed for development and benchmarking of novel graph neural networks (GNNs). The original OGB-LSC 2021 competition motivated a wide range of solutions using both MPNNs and transformers. However, following the success of the winning method Graphomer (Ying et al., 2021a), subsequent work has resulted in a large number of graph transformer methods for this task with comparatively little attention given to the message passing methods that have been successful in other graph-structured tasks.

In this work we build on the work of Rampášek et al. (2022) that advocates for a hybrid approach, including both message passing and transformer components in their General, Powerful, Scalable (GPS) framework. Specifically, we build GPS++, which combines a large and expressive message-passing module with a biased self-attention layer to maximise the benefit of local inductive biases while still allowing for effective global communication. Furthermore, by integrating a grouped input masking method (Luo et al., 2022) to exploit available 3D positional information, carefully crafting a range of diverse input features, and building a large ensemble we achieve the best-reported result on the PCQM4Mv2 test-challenge data split of 71.9 meV mean absolute error (MAE).

Next, we perform an extensive ablation study to understand the impact of different model components on the performance. Surprisingly, we find that even without a global self-attention mechanism (seen in graph transformer architectures), competitive performance can be achieved.

Therefore, we argue that MPNNs remain competitive in the molecular property prediction task and hope the results presented in this work can spark a renewed interest in this area. We also observe that when solely focusing on 2D molecular data (without 3D conformer coordinates), our proposed GPS++ model significantly outperforms other such works.

Our contributions can be summarised as follows:

- We show that our hybrid MPNN/Transformer model, GPS++, is a parameter-efficient and effective approach to molecular property prediction, achieving lower MAE for PCQM4Mv2 compared to models of similar size and comparable to the best-reported error for larger models.
- We find that even without self-attention, our model is competitive with prior state-of-the-art transformers, highlighting that well-optimised MPNNs are still highly effective in this domain.
- We investigate how different model components affect the model performance, in particular highlighting the impact of the improved chemical feature choice, 3D positional features and architectural components.
- We show that a large diverse ensemble of GPS++ models achieves a test MAE result on PCQM4Mv2 that is the state-of-the-art at time of submission (Table 1).

Reproducibility: Source code to reproduce our results can be found at: <https://github.com/graphcore/ogb-lsc-pcqm4mv2>.

2. Related Work

Before the advent of deep learning for graph representation learning (Bronstein et al., 2021), molecular representation in chemoinformatics rested on feature engineering of descriptors or fingerprints (Rogers & Hahn, 2010; Keith et al., 2021). After learnable fingerprints (Duvenaud et al., 2015) the general framework of GNNs, often based on MPNNs, has been rapidly gaining adoption (Reiser et al., 2022).

GNN method development has also been facilitated by the availability of well motivated (suites of) benchmarking datasets such as QM9 (Ramakrishnan et al., 2014), MoleculeNet (Wu et al., 2018), Open Graph Benchmark (OGB) (Hu et al., 2020), OGB-LSC PCQM4Mv2 (Hu et al., 2021), Therapeutics Data Commons (Huang et al., 2022) for molecular property prediction or MD17 (Chmiela et al., 2017), ANI-1 (Smith et al., 2017), Open Catalyst (Tran et al., 2022) for structural conformers or molecular force field predictions.

In this work we are primarily motivated by the PCQM4Mv2 dataset that is a part of the large-scale graph ML challenge (Hu et al., 2021), contains uniquely large numbers of graphs, and has the particular characteristic that the molecular 3D structure is only provided for the training portion of the dataset, but not at test time. This has motivated methods specifically equipped to handle such a scenario: Noisy Nodes denoising autoencoding (Godwin et al., 2022) and pretraining (Zaidi et al., 2022), GEM-2 (Liu et al., 2022), ViSNet (Wang et al., 2022b). Methods based on global self-attention (Vaswani et al., 2017) became particularly dominant after Graphomer (Ying et al., 2021a) won OGB-LSC 2021, which spurred development of transformer-based methods: SAN (Kreuzer et al., 2021), EGT (Hussain et al., 2022), GPS (Rampášek et al., 2022), TokenGT (Kim et al., 2022), or Transformer-M (Luo et al., 2022), that have superseded message-passing GNNs.

3. Preliminaries

Throughout the paper we use the following notation. Bold lowercase letters \mathbf{v} are (row) vectors, bold uppercase letters \mathbf{M} are matrices, with individual elements denoted by non-bold letters i.e. v_k or M_{pq} . Blackboard bold lowercase letters \mathbf{v} are categorical (integer-valued) vectors. In general, we denote by $[\mathbf{v}_k]_{k \in K}$ the vertical concatenation (stacking) of vectors \mathbf{v}_k . Vertical concatenation is also denoted by a semicolon, i.e. $[\mathbf{v}_1 ; \dots ; \mathbf{v}_J] = [\mathbf{v}_j]_{j=1}^J = [\mathbf{v}_j \text{ for } j \in \{1..J\}]$. Horizontal concatenation, which typically means concatenation along the feature dimension, is denoted by a vertical bar, i.e. $[\mathbf{v}_1 \mid \mathbf{v}_2]$.

A molecule is represented as a graph $\mathcal{G} = (\mathcal{V}, \mathcal{E})$ for nodes \mathcal{V} and edges \mathcal{E} . In this representation, each node $i \in \mathcal{V}$ is an atom in the molecule and each edge $(u, v) \in \mathcal{E}$ is a

chemical bond between two atoms. The number of atoms in the molecule is denoted by $N = |\mathcal{V}|$ and the number of edges is $M = |\mathcal{E}|$.

Each node and edge is associated with a list of categorical features $\mathbf{x}_i \in \mathbb{Z}^{D_{\text{atom}}}$ and $\mathbf{e}_{uv} \in \mathbb{Z}^{D_{\text{bond}}}$, respectively, for D_{atom} atom features and D_{bond} bond features. A further set of 3D atom positions $\mathbf{R} = [\mathbf{r}_1 ; \dots ; \mathbf{r}_N] \in \mathbb{R}^{N \times 3}$, extracted from original DFT calculations, is provided for training data, but crucially not for validation and test data.

Our algorithm operates on edge, node, and global *features*. Node features in layer ℓ are denoted by $\mathbf{x}_i^\ell \in \mathbb{R}^{d_{\text{node}}}$, and are concatenated into the $N \times d_{\text{node}}$ matrix $\mathbf{X}^\ell = [\mathbf{x}_1^\ell ; \dots ; \mathbf{x}_N^\ell]$. Edge features $\mathbf{e}_{uv}^\ell \in \mathbb{R}^{d_{\text{edge}}}$ are concatenated into the edge feature matrix $\mathbf{E}^\ell = [\mathbf{e}_{uv}^\ell \text{ for } (u, v) \in \mathcal{E}]$. Global features are defined per layer as $\mathbf{g}^\ell \in \mathbb{R}^{d_{\text{global}}}$.

We also define an *attention bias* matrix $\mathbf{B} \in \mathbb{R}^{N \times N}$, computed from the input graph topology and 3D atom positions, described later in §4.2.

4. GPS++

Our GPS++ model closely follows the GPS framework set out by Rampášek et al. (2022). This work presents a flexible model structure for building hybrid MPNN/Transformer models for graph-structured input data. We build a specific implementation of GPS that focuses on maximising the benefit of the inductive biases of the graph structure and 3D positional information. We do this by building a large and expressive MPNN component and biasing our attention component with structural and positional information. We also allow global information to be propagated through two mechanisms, namely the global attention and by using a global feature in the MPNN.

The main GPS++ block (§4.1) combines the benefits of both message passing and attention layers by running them in parallel before combining them with a simple summation and MLP; this layer is repeated 16 times. This main trunk of processing is preceded by an Encoder function responsible for encoding the input information into the latent space (§4.2), and is followed by a simple Decoder function (§5.2).

Feature engineering is also used to improve the representation of the atoms/bonds, to provide rich positional and structural features that increase expressivity, and to bias the attention weights with a distance embedding.

4.1. GPS++ Block

The GPS++ block is defined as follows for layers $\ell > 0$ (see §4.2 for the definitions of $\mathbf{X}^0, \mathbf{E}^0, \mathbf{g}^0, \mathbf{B}$):

$$\mathbf{X}^{\ell+1}, \mathbf{E}^{\ell+1}, \mathbf{g}^{\ell+1} = \text{GPS}^+(\mathbf{X}^\ell, \mathbf{E}^\ell, \mathbf{g}^\ell, \mathbf{B}) \quad (1)$$

computed as

$$\mathbf{Y}^\ell, \mathbf{E}^{\ell+1}, \mathbf{g}^{\ell+1} = \text{MPNN}(\mathbf{X}^\ell, \mathbf{E}^\ell, \mathbf{g}^\ell), \quad (2)$$

$$\mathbf{Z}^\ell = \text{BiasedAttn}(\mathbf{X}^\ell, \mathbf{B}), \quad (3)$$

$$\forall i : \mathbf{x}_i^{\ell+1} = \text{FFN}(\mathbf{y}_i^\ell + \mathbf{z}_i^\ell) \quad (4)$$

Our MPNN module is a variation on the neural message passing module with edge and global features (Gilmer et al., 2017; Battaglia et al., 2018; Bronstein et al., 2021). We choose this form to maximise the expressivity of the model with the expectation that overfitting will be less of an issue with PCQM4Mv2, compared to other molecular datasets, due to its size. The essential components (excluding dropout and layer norm) of the MPNN module are defined as follows (see Figure 2 for a graphical representation, and Appendix A.1 for the exact formulation):

$$\mathbf{Y}^\ell, \mathbf{E}^{\ell+1}, \mathbf{g}^{\ell+1} = \text{MPNN}(\mathbf{X}^\ell, \mathbf{E}^\ell, \mathbf{g}^\ell), \quad (5)$$

computed as

$$\forall (u, v) : \bar{\mathbf{e}}_{uv}^\ell = \text{MLP}_{\text{edge}} \left([\mathbf{x}_u^\ell | \mathbf{x}_v^\ell | \mathbf{e}_{uv}^\ell | \mathbf{g}^\ell] \right) \quad (6)$$

$$\forall i : \mathbf{c}_i^\ell = \left[\mathbf{x}_i^\ell \left| \sum_{(u, i) \in \mathcal{E}} \bar{\mathbf{e}}_{ui}^\ell \right| \sum_{(i, v) \in \mathcal{E}} \bar{\mathbf{e}}_{iv}^\ell \left| \sum_{(u, i) \in \mathcal{E}} \mathbf{x}_u^\ell \right| \mathbf{g}^\ell \right] \quad (7)$$

$$\forall i : \bar{\mathbf{x}}_i^\ell = \text{MLP}_{\text{node}}(\mathbf{c}_i^\ell) \quad (8)$$

$$\bar{\mathbf{g}}^\ell = \text{MLP}_{\text{global}} \left(\left[\mathbf{g}^\ell \left| \sum_{j \in \mathcal{V}} \bar{\mathbf{x}}_j^\ell \right| \sum_{(u, v) \in \mathcal{E}} \bar{\mathbf{e}}_{uv}^\ell \right] \right) \quad (9)$$

$$\forall i : \mathbf{y}_i^\ell = \bar{\mathbf{x}}_i^\ell + \mathbf{x}_i^\ell \quad (10)$$

$$\forall (u, v) : \mathbf{e}_{uv}^{\ell+1} = \bar{\mathbf{e}}_{uv}^\ell + \mathbf{e}_{uv}^\ell \quad (11)$$

$$\mathbf{g}^{\ell+1} = \bar{\mathbf{g}}^\ell + \mathbf{g}^\ell. \quad (12)$$

The three networks MLP_η for $\eta \in \{\text{node}, \text{edge}, \text{global}\}$ each have two layers with GELU activation functions and an expanded intermediate hidden dimension of $4d_\eta$.

This message passing block is principally the most similar to Battaglia et al. (2018). However we draw the reader’s attention to a few areas that differ from common approaches. First we aggregate over the adjacent node representations as well as the more complex edge feature messages in Equation 7, this is similar to running a simple graph convolutional network (GCN) in parallel to the more complex message calculation. We also aggregate over both sender and receiver edges but critically concatenate rather than sum the results to maintain some degree of directionality. Finally, we choose to decouple the three latent sizes, setting $d_{\text{node}} = 256$, $d_{\text{edge}} = 128$ and $d_{\text{global}} = 64$. While the primary reason is that, empirically, we find increasing d_{edge}

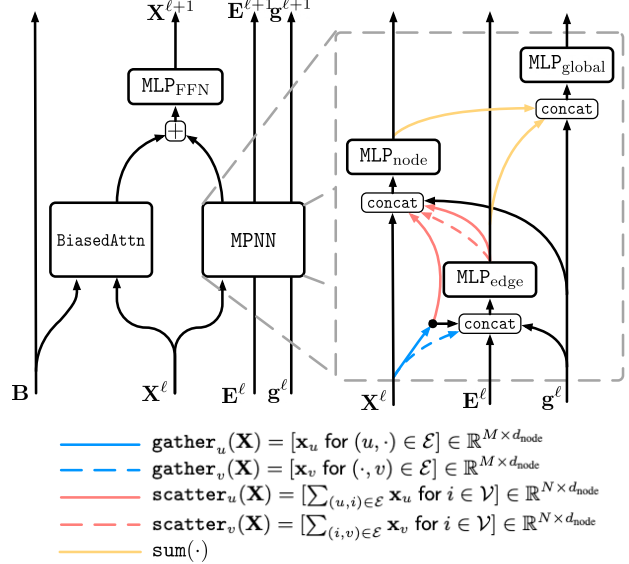


Figure 2. The main GPS++ processing block (left) is composed of a local message passing MPNN module and a biased global attention BiasedAttn module. (right) A diagram of the used MPNN block. The gather, scatter and sum operations highlight changes in tensor shapes and are defined as above.

and d_{global} does not improve performance, this choice also leads to greater efficiency.

Our BiasedAttn module follows the form of the self-attention layer of Luo et al. (2022) where a standard self-attention block (Vaswani et al., 2017) is biased by a structural prior derived from the input data. In our work, the bias \mathbf{B} is made up of two components, a shortest path distance (SPD) embedding and a 3D distance bias derived from the molecular conformations as described in §4.2. The FFN module takes a similar form to MLP_{node} though with additional dropout terms (see Appendix A.1 for full details).

4.2. Input Feature Engineering

As described in §3, the dataset samples include the graph structure \mathcal{G} , a set of categorical features for the atoms and bonds \mathbf{x}_i , \mathbf{e}_{uv} , and the 3D node positions \mathbf{r}_i . It has been shown that there are many benefits to augmenting the input data with additional structural, positional, and chemical information (Rampášek et al., 2022; Wang et al., 2022a; Dwivedi et al., 2022). Therefore, we combine several feature sources when computing the input to the first GPS++ layer. There are four feature tensors to initialise; node state, edge state, whole graph state and attention biases.

$$\mathbf{X}^{\text{all}} = [\mathbf{X}_{\text{atom}} | \mathbf{X}^{\text{LapVec}} | \mathbf{X}^{\text{LapVal}} | \mathbf{X}^{\text{RW}} | \mathbf{X}^{\text{Cent}} | \mathbf{X}^{\text{3D}}]$$

$$\mathbf{X}^0 = \text{Dense}(\mathbf{X}^{\text{all}}) \in \mathbb{R}^{N \times d_{\text{node}}} \quad (13)$$

$$\mathbf{E}^0 = \text{Dense}([\mathbf{E}^{\text{bond}} | \mathbf{E}^{\text{3D}}]) \in \mathbb{R}^{M \times d_{\text{edge}}} \quad (14)$$

$$\mathbf{g}^0 = \text{Embed}_{d_{\text{global}}}(0) \in \mathbb{R}^{d_{\text{global}}} \quad (15)$$

$$\mathbf{B} = \mathbf{B}^{\text{SPD}} + \mathbf{B}^{\text{3D}} \in \mathbb{R}^{N \times N} \quad (16)$$

Here the node features \mathbf{X}^0 are built from categorical atom features, graph Laplacian positional encodings (Kreuzer et al., 2021; Dwivedi & Bresson, 2020), random walk structural encodings (Dwivedi et al., 2022), local graph centrality encodings (Ying et al., 2021a; Shi et al., 2022) and a 3D centrality encoding (Luo et al., 2022). The edge features \mathbf{E}^0 are derived from categorical bond features and bond lengths, and the attention bias uses SPD and 3D distances. These input features are further described in Appendix A.2.

Chemical Features The categorical features \mathbf{x}, \mathbf{e} encapsulate the known chemical properties of the atoms and bonds, for example, the atomic number, the bond type or the number of attached hydrogens (which are not explicitly modelled as nodes), as well as graphical properties like node degree or whether an atom or bond is within a ring. The set that is used is not determined by the dataset and augmenting or modifying the chemical input features is a common strategy for improving results.

By default, the PCQM4Mv2 dataset uses a set of 9 atom and 3 bond features (described in Table A.1). There is, however, a wide range of chemical features that can be extracted from the periodic table or using tools like RDKit. Ying et al. (2021b) have shown that extracting additional atom level properties can be beneficial when trying to predict the HOMO-LUMO energy gap, defining a total of 28 atom and 5 bond features. We explore the impact of a number of additional node and edge features and sweep a wide range of possible combinations.

In particular, we expand on the set defined by Ying et al. (2021b) with three additional atom features derived from the periodic table, the atom group (column), period (row) and element type (often shown by colour). We found that these three additional features were particularly beneficial.

We also found that in many cases *removing* features was beneficial, for example, we found that all our models performed better when excluding information about chiral tag and replacing it with chiral centers. We further observe that our best feature combinations all consist of only 8 node features, where the majority of the input features stay consistent between the sets. We show the three best feature sets found in Table A.1 and use *Set 1* for all experiments unless otherwise stated (e.g., during ablations and ensembling).

5. Experimental Setup

5.1. Dataset

The PCQM4Mv2 dataset (Hu et al., 2021) consists of 3.7M molecules defined by their SMILES strings. Each molecule

has on average 14 atoms and 15 chemical bonds. However, as the bonds are undirected in nature and graph neural networks act on directed edges, two bidirectional edges are used to represent each chemical bond.

The 3.7M molecules are separated into standardised sets by OGB (Hu et al., 2021), namely into **training** (90%), **validation** (2%), **test-dev** (4%) and **test-challenge** (4%) sets using a scaffold split where the HOMO-LUMO gap targets are only publicly available for the **training** and **validation** splits.

5.2. Model Training

Training Configuration Our model training setup uses the Adam optimiser (Kingma & Ba, 2015) with a gradient clipping value of 5, a peak learning rate of 4e-4 and the model is trained for a total of 450 epochs. We used a learning rate warmup period of 10 epochs followed by a linear decay schedule.

Decoder and Loss The final model prediction is formed by global sum-pooling of all node representations and then passing it through a 2-layer MLP. The regression loss is the mean absolute error (L1 loss) between a scalar prediction and the ground truth HOMO-LUMO gap value.

Noisy Nodes/Edges Noisy nodes (Godwin et al., 2022; Zaidi et al., 2022) has previously been shown to be beneficial for molecular GNNs including on the PCQM4M dataset. The method adds noise to the input data then tries to reconstruct the uncorrupted data in an auxiliary task. Its benefits are expected to be two-fold: it adds regularisation by inducing some noise on the input, but also combats oversmoothing by forcing the node-level information to remain discriminative throughout the model. This has been shown to be particularly beneficial when training deep GNNs (Godwin et al., 2022). We follow the method of Godwin et al. (2022) that applies noise to the categorical node features by randomly choosing a different category with probability p_{corrupt} , and we further extend this to the categorical edge features. A simple categorical cross-entropy loss is then used to reconstruct the uncorrupted features at the output. We set $p_{\text{corrupt}} = 0.01$ and weight the cross-entropy losses such that they have a ratio 1:1.2:1.2 for losses HOMO-LUMO:NoisyNodes:NoisyEdges.

Grouped Input Masking The 3D positional features \mathbf{R} are only defined for the training data. We must therefore make use of them in training without requiring them for validation/test. We found that the method proposed by Luo et al. (2022) achieved the most favourable results so we adopt a variation hereon referred to as *grouped input masking*.

Atom distances calculated from 3D positions are embedded into vector space \mathbb{R}^K via $K = 128$ Gaussian kernel func-

Table 2. Comparison of single model performance on PCQM4Mv2 dataset. Note Transformer-M and Global-ViSNet are concurrent work.

Model	# Param.	Model Type	Valid. MAE (meV) ↓
<i>without 3D Positional Information</i>			
GCN-virtual (Hu et al., 2021)	4.9M	MPNN	115.3
GIN-virtual (Hu et al., 2021)	6.7M	MPNN	108.3
GRPE (Park et al., 2022)	46.2M	Transformer	89.0
Transformer-M (Medium, No 3D Positions) (Luo et al., 2022)	47.1M	Transformer	87.8
EGT (Hussain et al., 2022)	89.3M	Transformer	86.9
Graphomer (Shi et al., 2022)	48.3M	Transformer	86.4
GPS (Rampášek et al., 2022)	19.4M	Hybrid	85.8
GPS++ (No 3D Positions)	44.3M	Hybrid	82.0
GPS++ (No MHSA, No 3D Positions)	40.0M	MPNN	81.0
<i>with 3D Positional Information</i>			
Transformer-M (Medium, No Denoising) (Luo et al., 2022)	47.1M	Transformer	81.1
GEM-2 (Liu et al., 2022)	32.1M	Transformer	79.3
Transformer-M (Medium) (Luo et al., 2022)	47.1M	Transformer	78.7
GPS++ (No MHSA)	40.0M	MPNN	78.6
Global-ViSNet (Wang et al., 2022b)	78.5M	Transformer	78.4
GPS++	44.3M	Hybrid	77.8
Transformer-M (Large) (Luo et al., 2022)	69.0M	Transformer	77.2

tions. We then process these distance embeddings in three ways to produce attention biases (\mathbf{B}^{3D}), node features (\mathbf{X}^{3D}) and edge features (\mathbf{E}^{3D}) (exact formulations can be found in Appendix A.2).

This method stochastically masks out any features derived from the 3D positional features \mathbf{R} to build robustness to their absence. Specifically, this is done by defining two input sets to be masked:

$$\mathcal{X}^{\text{Spatial}} = \{\mathbf{X}^{3D}, \mathbf{E}^{3D}, \mathbf{B}^{3D}\}, \quad \mathcal{X}^{\text{Topological}} = \{\mathbf{B}^{\text{SPD}}\}$$

and three potential masking groups: 1. Mask $\mathcal{X}^{\text{Spatial}}$, 2. Mask $\mathcal{X}^{\text{Topological}}$, and 3. No masking. These masking groups are then sampled randomly throughout training with ratio 1:3:1. If 3D positions are not defined, e.g. in validation/test, masking group 1 is always used.

Training Time Our GPS++ model trains at 17,500 graphs per second on 16 IPUs which means each epoch completes in 3 minutes and a full 450 epoch training run takes 24 hours. Full details of the hardware used and acceleration methods employed can be found in Appendix B.

6. Results

Single Model Performance In Table 2, we compare the single model performance of GPS++ with results from the literature, in particular, we pay close attention to the Transformer-M (Luo et al., 2022) model as it has the best results for a transformer, but also because we use their input masking method for incorporating 3D features; this allows us to gain some tangible insights into the value of hybrid/MPNN approaches vs. transformer.

Comparing the best GPS++ result with prior work, we see improvement over all results apart from the largest Transformer-M that is only narrowly better, however, we see

that GPS++ overtakes the Transformer-M with comparable parameters. Another interesting feature of the Transformer-M is that it implements a 3D denoising loss, not present in GPS++ due to Transformer-M being released towards the end of GPS++ development, which achieves a significant performance boost. Without this feature, in a regime more similar to ours, we see a significant performance reduction in Transformer-M relative to GPS++.

While it would be tempting to assume that the attention element of our model is the most significant due to the prevalence of transformers among the other top results, we find that we can maintain a large proportion of the accuracy with no attention at all, falling back to a pure MPNN, passing messages only between bonded atoms (nodes). Furthermore, we show that this MPNN model is more accurate in the absence of 3D features, even beating the hybrid GPS++ in this setting. We believe this shows a strong reliance of global attention mechanisms on 3D positional information and, in contrast, the power of using message passing along molecular bonds. We further investigate the impact of different elements of the model in §7.

Ensembled Model Performance To test our GPS++ model on the official PCQM4Mv2 test set we build a large ensemble to maximise the model accuracy. For this we focus on both the size of ensemble as well as the diversity which are both well-known factors for achieving good ensemble performance (Zhou et al., 2002; Lakshminarayanan et al., 2017). Furthermore, as we are aiming to infer the model on the test-challenge set we also include the validation set in training. The strategy taken to build the ensemble is outlined in Appendix C. In the end we build an ensemble of 112 models using 7 different configurations of GPS++ which achieves a final test-challenge MAE of 71.9 meV that beats all prior work on this dataset (see Table 1). Inference

was completed in 1 hour 32 minutes using 1 IPU and AMD EPYC 7742 64-Core CPU, including all the feature processing and program compilation, which is well under the 4 hour constraint typically applied to this task.

7. Ablation Study

The top-performing GPS++ model was attained empirically, resulting in a complex combination of input features, architectural choices and loss functions. In this section we assess the contribution of each feature to final task performance on PCQM4Mv2, and find that much of the performance can be retained by a simplified design. All results listed in the ablation study are obtained by training the final GPS++ model from scratch for 200 epochs with one or more features disabled, averaging MAE over 5 runs.

Node and Edge Input Features The PCQM4Mv2 dataset provides 9 chemical node and 3 edge features for each sample, and following prior work GPS++ incorporates additional features and preprocessing strategies. Table 3 isolates the contribution of each of these additions (excluding 3D features).

Table 3. Ablation of node and edge features.

Removed Feature	Δ MAE (meV)	
	Valid	Train
None (Baseline)	78.4	52.3
Random Walk Structural Enc	+ 1.3	+ 1.3
Laplacian Positional Enc	- 0.1	- 0.3
Local Centrality Enc	0.0	+ 0.6
Bond Lengths	0.0	- 0.4
Noisy Edges	+ 0.1	- 0.2
Noisy Nodes	+ 0.5	+ 0.3

In line with previous work (Rampášek et al., 2022), the Random Walk Structural Encoding is the most impactful individual input feature, degrading validation performance by 1.3meV upon removal, whilst the Graph Laplacian Positional Encodings (both eigenvectors and eigenvalues) are found to have no benefit. Other features, despite being beneficial when they were added at intermediate steps in the development of the model, are shown to have become similarly redundant in the final GPS++ composition: the Graphomer-style Local Centrality Encoding (i.e. embedding the degree of the node) carries no information that the Random Walks do not, and the use of Bond Lengths as an edge feature in the MPNN appears to be unnecessary in the presence of more comprehensive 3D features elsewhere in the network. Though both features are equally redundant for task performance, the "2D" graph Centrality Encoding is contributing much more to overfitting than the "3D" Bond Length, a pattern that is evident elsewhere in the ablations. Table 3 also shows that whilst the regularisation effect of the noisy nodes loss is beneficial, the contribution of noisy

Table 4. Choices of chemical features.

Feature Set	Atom Group, Period & Type	Set Size	Δ MAE (meV)	
			Valid	Train
Set 1 (Baseline)	✓	14	78.4	52.3
Set 2	✓	14	- 0.1	+ 0.0
Set 3	✓	14	- 0.1	- 0.2
Set 1	.	11	+ 0.5	- 0.4
Original	✓	15	+ 1.2	+ 0.1
Original	.	12	+ 1.7	+ 0.5
Ying21	✓	36	+ 5.4	- 5.2
Ying21	.	33	+ 5.0	- 4.4

edges is negligible. This may be due to the simplicity (and hence ease of denoising) of the limited edge features in PCQM4Mv2.

Table 4 compares the possible choices of chemical input features described in §4.2: *Original* is the set of features included in PCQM4Mv2; *Ying21* refers to all 28 node features and 5 edge features in the PCQ superset defined by Ying et al. (2021b); *Set 1-3* are performant subsets of 11 node features and 3 edge features selected from all of the above, defined fully in Table A.1 and obtained via a combinatorial search; *Atom Group, Period & Type* refers to our contribution of 3 additional atom features relating to an atom's position in the periodic table, intended to be more generalised than the atomic number. The results clearly show that training on all 36 available input features causes significant overfitting and degrades task performance by introducing noise. Moreover, the original PCQM4Mv2 features are not an optimal subset; the significant difference between *Original* and *Set 1* is largely due to the removal of the original Chiral Tag feature, which has been replaced by a Chiral Center boolean. Lastly, the table shows that *Atom Group, Period & Type* provide meaningfully richer information than the atomic number feature which is present in every feature set, but are not immune to exacerbating overfitting in cases where too many features are used.

3D Input Features and MHSA The 3D node position information given for the training set in PCQM4Mv2 is provided as input to the final model in two forms: the all-to-all 3D Bias map added to the self-attention module, and the node-wise 3D Centrality Encoding added in the encoder. The first four rows of Table 5 show that they both improve task performance independently and in combination, but to different degrees. Whilst the 3D Bias is meaningfully beneficial to the valid MAE, the 3D Centrality has a greater impact and is also responsible for a significant reduction in overfitting visible in the training MAE, suggesting improved generalisation capabilities. Additionally, we found that training stability of the MHSA module suffered in the absence of either 3D feature, requiring us to halve the learning rate to 2e-4 for convergence unless the MHSA module was disabled.

Table 5. Ablation of self-attention and 3D features.

#	Feature				Δ MAE (meV)	
	MHSA	SPD Bias	3D Bias	3D Centrality	Valid	Train
1	✓	✓	✓	✓	78.4	52.3
2	✓	✓	✓	.	+ 2.0	-8.4 *
3	✓	✓	.	✓	+ 0.9	-2.5 *
4	✓	✓	.	.	+ 3.6	-8.9 *
5	✓	.	.	.	+ 3.5	-8.2 *
6	+ 2.5	-9.9
7	✓	.	.	✓	+ 0.9	-1.8 *
8	.	.	.	✓	+ 0.9	-0.5
9	✓	.	✓	✓	+ 0.1	+0.3

* trained with half learning rate for stability

Interestingly, in the absence of both 3D features, Table 5 rows 4-6 show that it is preferable to *remove* the MHSA. Even with the 3D Centrality feature added to nodes in rows 7-8, a "standard" unbiased MHSA is not beneficial to task performance and increases overfitting. This implies that the Shortest Path Distance Bias term, which attempts to provide a non-3D global graph positional encoding to the MHSA, is insufficient to modulate attention between atoms, and that instead spatial relationships are key for this quantum chemistry task. Indeed, in rows 4 vs 5, 3 vs 7 and 1 vs 9 the SPD Bias is shown to increase overfitting whilst having a negligible valid MAE impact. This result stands out against previous work where the SPD Bias was an effective component of state-of-the-art graph transformers on PCQM4Mv2; one explanation may be that in the absence of an MPNN module graph transformers rely on the SPD Bias to identify neighbourhoods and recreate some of the functionality of MPNNs within the MHSA layer, as described in section 3.3 of Ying et al. (2021a).

Table 6. Ablation of network architecture features.

Removed Feature	Δ MAE (meV)		
	Valid	Train	Δ Param.
None (Baseline)	78.4	52.3	44.3M
MPNN	+ 13.3	+ 21.1	-69.8%
Edge Features	+ 4.4	+ 3.7	-26.3%
Global Features	+ 1.0	+ 0.4	- 8.0%
Sender Message Aggregation	+ 0.7	- 0.4	-14.2%
Adjacent Node Aggregation	+ 0.4	+ 2.1	-18.9%
MHSA	+ 0.9	- 0.5	- 9.5%
FFN	+ 0.8	+ 0.9	-19.0%
MHSA and Global Features	+ 3.5	+ 0.2	-17.5%

Model Architecture GPS++ uses a large MPNN module comprising 70% of the model parameters and using extensively tuned hyper-parameters. Table 6 ablates the components of the model network architecture, and shows that the MPNN module is unsurprisingly the single most important component for task performance. Outside of the MPNN, the MHSA (with accompanying attention biases) and FFN contribute approximately equally to the final performance,

though they have opposite impacts on training MAE. Within the MPNN, the largest task impact arises from removing the edge features and edge MLP from all layers (e_{uv} and MLP_{edge} in Equation 6), falling back on simple GCN-style message passing that concatenates neighbouring node features when computing messages. Table 6 also shows that the use of Adjacent Node Feature Aggregation (i.e., the sum of adjacent node features x_u^ℓ in Equation 7) allows large node features of size 256 to bypass compression into edge messages of size 128, affording a small but meaningful MAE improvement. It is likely due to this feature that we have not found a benefit to increasing the edge latent size to match the node size. Both the use of Global Features and Sender Message Aggregation within the MPNN are shown to be of comparable importance to the MHSA and FFN modules. Global Features, denoted as g^ℓ in Equation 6 and 7, allow the MPNN some degree of global reasoning, whilst Sender Message Aggregation (the sum of \bar{e}_{iv}^ℓ in Equation 7) uses outgoing messages in addition to the usual incoming messages to update a node's features. There is some overlap in purpose of the Global Features and the MHSA module, so the table also shows the impact of removing both at once. The resulting performance degradation is significantly greater than the sum of their individual impacts, which may imply each feature is able to partially compensate for the loss of the other in the individual ablations.

8. Discussion

In this work, we define GPS++, a hybrid MPNN/ Transformer, optimised for the PCQM4Mv2 molecular property prediction task (Hu et al., 2021). Our model builds on previous work (Rampášek et al., 2022; Luo et al., 2022; Godwin et al., 2022) with a particular focus on building a powerful and expressive message passing component. Despite strong trends to use transformers for molecular property prediction, we showed that our GPS++ model is very competitive with prior work achieving the best results when comparing similar sized models, only marginally worse than the best larger transformer model. To our surprise, we also found that without any global attention mechanism at all, GPS++ (now a pure MPNN) retains almost all of its performance. Finally, we consider the case where 3D positions are not available and show that our GPS++ models are significantly better than Transformers, where a significant drop-off is observed across all prior work. We also found that our MPNN-only model performs better than our hybrid under these circumstances, this indicates a strong reliance between effective attention and the availability of 3D positional information.

Finally, we built a large diverse ensemble of GPS++ models and achieved an MAE of 71.9 meV on the PCQM4Mv2 test-challenge set with four-hour inference time budget, the state-of-the-art at time of submission.

Whilst these results are interesting for problems with small

molecules, testing on much larger molecules, for example, peptides, proteins, or RNAs, which can have hundreds or thousands of atoms, is a tougher challenge. Under these conditions, the linear complexity of MPNNs with graph size suggests some computational benefits over global attention, however, it is still to be determined if the downsides of issues like underreaching outweigh these benefits. Nevertheless, we believe that our results highlight the strength of MPNNs in this domain and hope that it inspires a revival of message passing and hybrid models for molecular property prediction when dealing with large datasets.

References

Alon, U. and Yahav, E. On the bottleneck of graph neural networks and its practical implications. In *International Conference on Learning Representations*, 2021.

Axelrod, S. and Gomez-Bombarelli, R. Geom, energy-annotated molecular conformations for property prediction and molecular generation. *Scientific Data*, 9(1):1–14, 2022.

Ba, J. L., Kiros, J. R., and Hinton, G. E. Layer normalization. *arXiv:1607.06450*, 2016.

Battaglia, P. W., Hamrick, J. B., Bapst, V., Sanchez-Gonzalez, A., Zambaldi, V., Malinowski, M., Tacchetti, A., Raposo, D., Santoro, A., Faulkner, R., et al. Relational inductive biases, deep learning, and graph networks. *arXiv:1806.01261*, 2018.

Bilbrey, J. A., Herman, K. M., Sprueill, H., Xantheas, S. S., Das, P., Roldan, M. L., Kraus, M., Helal, H., and Choudhury, S. Reducing down(stream)time: Pretraining molecular gnns using heterogeneous ai accelerators. *arXiv preprint arXiv:2211.04598*, 2022.

Bronstein, M. M., Bruna, J., Cohen, T., and Veličković, P. Geometric deep learning: Grids, groups, graphs, geodesics, and gauges. *arXiv:2104.13478*, 2021.

Chmiela, S., Tkatchenko, A., Sauceda, H. E., Poltavsky, I., Schütt, K. T., and Müller, K.-R. Machine learning of accurate energy-conserving molecular force fields. *Science advances*, 3(5):e1603015, 2017.

Darabi, S., Fazeli, S., Liu, J., Milesi, A., Morkisz, P., Puget, J.-F., and Titericz, G. Heterogeneous ensemble of models for molecular property prediction. https://https://ogb.stanford.edu/paper/neurips2022/pcqm4mv2_NVIDIA-PCQM4Mv2.pdf, 2022. Accessed: 2023-01-24.

Dobson, C. M. Chemical space and biology. *Nature*, 432(7019):824–828, December 2004. ISSN 1476-4687. doi:10.1038/nature03192.

Duvenaud, D. K., Maclaurin, D., Iparraguirre, J., Bombarell, R., Hirzel, T., Aspuru-Guzik, A., and Adams, R. P. Convolutional networks on graphs for learning molecular fingerprints. *Advances in neural information processing systems*, 28, 2015.

Dwivedi, V. P. and Bresson, X. A generalization of transformer networks to graphs. *arXiv:2012.09699*, 2020.

Dwivedi, V. P., Luu, A. T., Laurent, T., Bengio, Y., and Bresson, X. Graph neural networks with learnable structural and positional representations. In *International Conference on Learning Representations*, 2022.

Fey, M. and Lenssen, J. E. Fast graph representation learning with PyTorch Geometric. In *ICLR Workshop on Representation Learning on Graphs and Manifolds*, 2019.

Gilmer, J., Schoenholz, S. S., Riley, P. F., Vinyals, O., and Dahl, G. E. Neural message passing for quantum chemistry. In *International conference on machine learning*, pp. 1263–1272. PMLR, 2017.

Godwin, J., Schaarschmidt, M., Gaunt, A. L., Sanchez-Gonzalez, A., Rubanova, Y., Veličković, P., Kirkpatrick, J., and Battaglia, P. Simple GNN regularisation for 3D molecular property prediction and beyond. In *International Conference on Learning Representations*, 2022.

Hendrycks, D. and Gimpel, K. Gaussian error linear units (GELUs). *arXiv:1606.08415*, 2016.

Hu, W., Fey, M., Zitnik, M., Dong, Y., Ren, H., Liu, B., Catasta, M., and Leskovec, J. Open Graph Benchmark: Datasets for Machine Learning on Graphs. *34th Conference on Neural Information Processing Systems*, 2020.

Hu, W., Fey, M., Ren, H., Nakata, M., Dong, Y., and Leskovec, J. OGB-LSC: A large-scale challenge for machine learning on graphs. In *35th Conference on Neural Information Processing Systems: Datasets and Benchmarks Track*, 2021.

Huang, G., Sun, Y., Liu, Z., Sedra, D., and Weinberger, K. Q. Deep networks with stochastic depth. In Leibe, B., Matas, J., Sebe, N., and Welling, M. (eds.), *Computer Vision – ECCV 2016*, pp. 646–661, Cham, 2016. Springer International Publishing. ISBN 978-3-319-46493-0.

Huang, K., Fu, T., Gao, W., Zhao, Y., Roohani, Y., Leskovec, J., Coley, C. W., Xiao, C., Sun, J., and Zitnik, M. Artificial intelligence foundation for therapeutic science. *Nature Chemical Biology*, 18(10):1033–1036, 2022.

Huang, Y., Cheng, Y., Bapna, A., Firat, O., Chen, M. X., Chen, D., Lee, H., Ngiam, J., Le, Q. V., Wu, Y., and Chen, Z. Gpipe: Efficient training of giant neural networks using pipeline parallelism. *arXiv preprint arXiv:1811.06965*, 2018.

Hussain, M. S., Zaki, M. J., and Subramanian, D. Global self-attention as a replacement for graph convolution. In *Proceedings of the 28th ACM SIGKDD Conference on Knowledge Discovery and Data Mining*, pp. 655–665, 2022.

Keith, J. A., Vassilev-Galindo, V., Cheng, B., Chmiela, S., Gastegger, M., Müller, K.-R., and Tkatchenko, A. Combining machine learning and computational chemistry for predictive insights into chemical systems. *Chemical Reviews*, 121(16):9816–9872, 2021. doi:[10.1021/acs.chemrev.1c00107](https://doi.org/10.1021/acs.chemrev.1c00107). PMID: 34232033.

Kim, J., Nguyen, T. D., Min, S., Cho, S., Lee, M., Lee, H., and Hong, S. Pure transformers are powerful graph learners. In *NeurIPS*, 2022.

Kingma, D. P. and Ba, J. Adam: A method for stochastic optimization. In *ICLR (Poster)*, 2015. URL <http://arxiv.org/abs/1412.6980>.

Kohn, W. and Sham, L. J. Self-consistent equations including exchange and correlation effects. *Phys. Rev.*, 140: A1133–A1138, Nov 1965.

Krell, M. M., Kosec, M., Perez, S. P., and Fitzgibbon, A. Efficient sequence packing without cross-contamination: Accelerating large language models without impacting performance. *arXiv preprint arXiv:2107.02027*, 2021.

Kreuzer, D., Beaini, D., Hamilton, W. L., Létourneau, V., and Tossou, P. Rethinking graph transformers with spectral attention. In *Advances in Neural Information Processing Systems*, 2021.

Lakshminarayanan, B., Pritzel, A., and Blundell, C. Simple and scalable predictive uncertainty estimation using deep ensembles. *Advances in neural information processing systems*, 30, 2017.

Li, Q., Han, Z., and Wu, X. Deeper insights into graph convolutional networks for semi-supervised learning. In *AAAI*, pp. 3538–3545, 2018.

Liu, L., He, D., Fang, X., Zhang, S., Wang, F., He, J., and Wu, H. GEM-2: Next generation molecular property prediction network with many-body and full-range interaction modeling. *arXiv preprint arXiv:2208.05863*, 2022.

Luo, S., Chen, T., Xu, Y., Zheng, S., Liu, T.-Y., Wang, L., and He, D. One transformer can understand both 2D & 3D molecular data. *arXiv:2210.01765*, 2022.

Micikevicius, P., Narang, S., Alben, J., Diamos, G., Elsen, E., Garcia, D., Ginsburg, B., Houston, M., Kuchaiev, O., Venkatesh, G., and Wu, H. Mixed precision training. *arXiv preprint arXiv:1710.03740*, 2017.

Nakata, M. and Shimazaki, T. Pubchemqc project: a large-scale first-principles electronic structure database for data-driven chemistry. *Journal of chemical information and modeling*, 57(6):1300–1308, 2017.

Park, W., Chang, W., Lee, D., Kim, J., and won Hwang, S. GRPE: Relative positional encoding for graph transformer. *arXiv:2201.12787*, 2022.

Ramakrishnan, R., Dral, P. O., Rupp, M., and Von Lilienfeld, O. A. Quantum chemistry structures and properties of 134 kilo molecules. *Scientific data*, 1(1):1–7, 2014.

Rampášek, L., Galkin, M., Dwivedi, V. P., Luu, A. T., Wolf, G., and Beaini, D. Recipe for a General, Powerful, Scalable Graph Transformer. *arXiv:2205.12454*, 2022.

RDKit. RDKit: Open-source cheminformatics. <http://www.rdkit.org>. [Online].

Reiser, P., Neubert, M., Eberhard, A., Torresi, L., Zhou, C., Shao, C., Metni, H., van Hoesel, C., Schopmans, H., Sommer, T., et al. Graph neural networks for materials science and chemistry. *Communications Materials*, 3(1): 93, 2022.

Rogers, D. and Hahn, M. Extended-connectivity fingerprints. *Journal of chemical information and modeling*, 50 (5):742–754, 2010.

Shi, Y., Zheng, S., Ke, G., Shen, Y., You, J., He, J., Luo, S., Liu, C., He, D., and Liu, T.-Y. Benchmarking graphomer on large-scale molecular modeling datasets. *arXiv:2203.04810*, 2022.

Smith, J. S., Isayev, O., and Roitberg, A. E. Ani-1, a data set of 20 million calculated off-equilibrium conformations for organic molecules. *Scientific data*, 4(1):1–8, 2017.

Srivastava, N., Hinton, G., Krizhevsky, A., Sutskever, I., and Salakhutdinov, R. Dropout: a simple way to prevent neural networks from overfitting. *The journal of machine learning research*, 15(1):1929–1958, 2014.

Tran, R., Lan, J., Shuaibi, M., Goyal, S., Wood, B. M., Das, A., Heras-Domingo, J., Kolluru, A., Rizvi, A., Shoghi, N., et al. The open catalyst 2022 (oc22) dataset and challenges for oxide electrocatalysis. *arXiv:2206.08917*, 2022.

Vaswani, A., Shazeer, N., Parmar, N., Uszkoreit, J., Jones, L., Gomez, A. N., Kaiser, Ł., and Polosukhin, I. Attention is all you need. *Advances in Neural Information Processing Systems*, 30, 2017.

Wang, H., Yin, H., Zhang, M., and Li, P. Equivariant and stable positional encoding for more powerful graph neural networks. In *International Conference on Learning Representations*, 2022a.

Wang, Y., Li, S., Wang, T., Wang, Z., He, X., Shao, B., and Liu, T.-Y. How to better introduce geometric information in equivariant message passing? https://github.com/ogb-visnet/Global-ViSNet/blob/master/ViSNet_Tech_Report.pdf, 2022b. Accessed: 2022-11-16.

Wang, Y., Li, S., Wang, T., Wang, Z., He, X., Shao, B., and Liu, T.-Y. An ensemble of VisNet, Transformer-M, and pretraining models for molecular property prediction in OGB Large-Scale Challenge @ NeurIPS 2022, 2022c.

Wu, Z., Ramsundar, B., Feinberg, E. N., Gomes, J., Gennesse, C., Pappu, A. S., Leswing, K., and Pande, V. Moleculenet: a benchmark for molecular machine learning. *Chemical science*, 9(2):513–530, 2018.

Ying, C., Cai, T., Luo, S., Zheng, S., Ke, G., He, D., Shen, Y., and Liu, T.-Y. Do transformers really perform badly for graph representation? In *Advances in Neural Information Processing Systems*, 2021a.

Ying, C., Yang, M., Zheng, S., Ke, G., Luo, S., Cai, T., Wu, C., Wang, Y., Shen, Y., and He, D. First place solution of KDD Cup 2021 & OGB large-scale challenge graph prediction track. *arXiv:2106.08279*, 2021b.

Zaidi, S., Schaarschmidt, M., Martens, J., Kim, H., Teh, Y. W., Sanchez-Gonzalez, A., Battaglia, P., Pascanu, R., and Godwin, J. Pre-training via denoising for molecular property prediction. *arXiv preprint arXiv:2206.00133*, 2022.

Zhou, Z.-H., Wu, J., and Tang, W. Ensembling neural networks: many could be better than all. *Artificial intelligence*, 137(1-2):239–263, 2002.

A. Detailed Model Description

A.1. GPS++ Block Complete

The GPS++ block is defined as follows for layers $\ell > 0$ (see §A.2 for the definitions of $\mathbf{X}^0, \mathbf{E}^0, \mathbf{g}^0$).

$$\mathbf{X}^{\ell+1}, \mathbf{E}^{\ell+1}, \mathbf{g}^{\ell+1} = \text{GPS++}(\mathbf{X}^\ell, \mathbf{E}^\ell, \mathbf{g}^\ell, \mathbf{B}) \quad (17)$$

computed as

$$\mathbf{Y}^\ell, \mathbf{E}^{\ell+1}, \mathbf{g}^{\ell+1} = \text{MPNN}(\mathbf{X}^\ell, \mathbf{E}^\ell, \mathbf{g}^\ell), \quad (18)$$

$$\mathbf{Z}^\ell = \text{BiasedAttn}(\mathbf{X}^\ell, \mathbf{B}), \quad (19)$$

$$\forall i: \mathbf{x}_i^{\ell+1} = \text{FFN}(\mathbf{y}_i^\ell + \mathbf{z}_i^\ell) \quad (20)$$

The MPNN module A simplified version of the MPNN module is presented in §4.1. The full description is as follows:

$$\mathbf{Y}^\ell, \mathbf{E}^{\ell+1}, \mathbf{g}^{\ell+1} = \text{MPNN}(\mathbf{X}^\ell, \mathbf{E}^\ell, \mathbf{g}^\ell), \quad (21)$$

computed as

$$\forall(u, v): \mathbf{c}_{uv}^\ell = [\mathbf{x}_u^\ell | \mathbf{x}_v^\ell | \mathbf{e}_{uv}^\ell | \mathbf{g}^\ell] \quad (22)$$

$$\forall(u, v): \bar{\mathbf{e}}_{uv}^\ell = \text{Dropout}_{0.0035}(\text{MLP}_{\text{edge}}(\mathbf{c}_{uv}^\ell)) \quad (23)$$

$$\forall i: \mathbf{c}_i^\ell = \left[\mathbf{x}_i^\ell \left| \sum_{(u, i) \in \mathcal{E}} \bar{\mathbf{e}}_{ui}^\ell \right. \right. \left| \sum_{(i, v) \in \mathcal{E}} \bar{\mathbf{e}}_{iv}^\ell \right. \left| \sum_{(u, i) \in \mathcal{E}} \mathbf{x}_u^\ell \right| \mathbf{g}^\ell \right] \quad (24)$$

$$\forall i: \bar{\mathbf{x}}_i^\ell = \text{MLP}_{\text{node}}(\mathbf{c}_i^\ell) \quad (25)$$

$$\bar{\mathbf{g}}^\ell = \text{MLP}_{\text{global}}\left(\left[\mathbf{g}^\ell \left| \sum_{j \in \mathcal{V}} \bar{\mathbf{x}}_j^\ell \right. \right. \left| \sum_{(u, v) \in \mathcal{E}} \bar{\mathbf{e}}_{uv}^\ell \right. \right] \right) \quad (26)$$

$$\forall i: \mathbf{y}_i^\ell = \text{LayerNorm}(\text{Dropout}_{0.3}(\bar{\mathbf{x}}_i^\ell) + \mathbf{x}_i^\ell) \quad (27)$$

$$\forall(u, v): \mathbf{e}_{uv}^{\ell+1} = \bar{\mathbf{e}}_{uv}^\ell + \mathbf{e}_{uv}^\ell \quad (28)$$

$$\mathbf{g}^{\ell+1} = \text{Dropout}_{0.35}(\bar{\mathbf{g}}^\ell) + \mathbf{g}^\ell, \quad (29)$$

where Dropout_p (Srivastava et al., 2014) masks by zero each element with probability p and LayerNorm follows the normalisation procedure of Ba et al. (2016). The three networks MLP_η for $\eta \in \{\text{node}, \text{edge}, \text{global}\}$ each have two layers and are defined by:

$$\mathbf{y} = \text{MLP}_\eta(\mathbf{x}) \quad (30)$$

$$\text{computed as } \bar{\mathbf{x}} = \text{GELU}(\text{Dense}(\mathbf{x})) \in \mathbb{R}^{4d_\eta} \quad (31)$$

$$\mathbf{y} = \text{Dense}(\text{LayerNorm}(\bar{\mathbf{x}})) \in \mathbb{R}^{d_\eta} \quad (32)$$

where GELU is from Hendrycks & Gimpel (2016).

The BiasedAttn module Our BiasedAttn module follows the form of the self-attention layer in Luo et al. (2022) where a standard self-attention block (Vaswani et al., 2017) is biased by a structural prior derived from the input graph. In our work the bias \mathbf{B} is made up of two components, a Shortest Path Distance embedding and a 3D Distance Bias derived from the molecular conformations as described in §A.2. Single-head biased attention is defined by:

$$\mathbf{Z} = \text{BiasedAttn}(\mathbf{X}, \mathbf{B}) \quad (33)$$

computed as

$$\mathbf{A} = \frac{(\mathbf{X}\mathbf{W}_Q)(\mathbf{X}\mathbf{W}_K)^\top}{\sqrt{d_{\text{node}}}} + \mathbf{B} \in \mathbb{R}^{N \times N} \quad (34)$$

$$\bar{\mathbf{A}} = \text{Dropout}_{0.3}(\text{Softmax}(\mathbf{A}))(\mathbf{X}\mathbf{W}_V) \in \mathbb{R}^{N \times d_{\text{node}}} \quad (35)$$

$$\mathbf{Z} = \text{GraphDropout}_{\frac{\ell}{L}0.3}(\bar{\mathbf{A}}) + \mathbf{X} \in \mathbb{R}^{N \times d_{\text{node}}} \quad (36)$$

for learnable weight matrices $\mathbf{W}_Q, \mathbf{W}_K, \mathbf{W}_V \in \mathbb{R}^{d_{\text{node}} \times d_{\text{node}}}$ and output in $\mathbb{R}^{N \times d_{\text{node}}}$, though in practice we use 32 attention heads which are mixed before GraphDropout using an affine projection $\mathbf{W}_P \in \mathbb{R}^{d_{\text{node}} \times d_{\text{node}}}$.

The FFN module Finally, the feed-forward network module takes the form:

$$\mathbf{y} = \text{FFN}(\mathbf{x}) \quad (37)$$

computed as

$$\bar{\mathbf{x}} = \text{Dropout}_p(\text{GELU}(\text{Dense}(\mathbf{x}))) \in \mathbb{R}^{4d_{\text{node}}} \quad (38)$$

$$\mathbf{y} = \text{GraphDropout}_{\frac{\ell}{L}0.3}(\text{Dense}(\bar{\mathbf{x}})) + \mathbf{x} \in \mathbb{R}^{d_{\text{node}}} \quad (39)$$

Unless otherwise stated, the dropout probability $p = 0$, however, we experiment with other values when ensembling multiple model variants. GraphDropout, also known as Stochastic Depth or LayerDrop (Huang et al., 2016), masks whole graphs together rather than individual nodes or features, relying on skip connections to propagate activations.

A.2. Input Feature Engineering

As described in §3, the dataset samples include the graph structure \mathcal{G} , a set of categorical features for the atoms and bonds $\mathbf{x}_i, \mathbf{e}_{uv}$, and the 3D node positions \mathbf{r}_i . It has been shown that there are many benefits to augmenting the input data with additional structural, positional, and chemical information (Rampášek et al., 2022; Wang et al., 2022a; Dwivedi et al., 2022). Therefore, we combine several feature sources when computing the input to the first GPS++ layer. There are four feature tensors to initialise; node state, edge state, whole graph state and attention biases.

$$\mathbf{X}^{\text{all}} = [\mathbf{X}^{\text{atom}} \mid \mathbf{X}^{\text{LapVec}} \mid \mathbf{X}^{\text{LapVal}} \mid \mathbf{X}^{\text{RW}} \mid \mathbf{X}^{\text{Cent}} \mid \mathbf{X}^{\text{3D}}] \quad (40)$$

$$\mathbf{X}^0 = \text{Dense}(\mathbf{X}^{\text{all}}) \in \mathbb{R}^{N \times d_{\text{node}}} \quad (41)$$

$$\mathbf{E}^0 = \text{Dense}([\mathbf{E}^{\text{bond}} \mid \mathbf{E}^{\text{3D}}]) \in \mathbb{R}^{M \times d_{\text{edge}}} \quad (42)$$

$$\mathbf{g}^0 = \text{Embed}_{d_{\text{global}}}(0) \in \mathbb{R}^{d_{\text{global}}} \quad (43)$$

$$\mathbf{B} = \mathbf{B}^{\text{SPD}} + \mathbf{B}^{\text{3D}} \in \mathbb{R}^{N \times N} \quad (44)$$

The various components of each of these equations are defined over the remainder of this section. The encoding of these features also makes recurring use of the following two generic functions. Firstly, a two-layer $\text{MLP}_{\text{encoder}}$ that projects features to a fixed-size latent space:

$$y = \text{MLP}_{\text{encoder}}(x), \quad \text{where } x \in \mathbb{R}^h \quad (45)$$

computed as

$$\bar{x} = \text{ReLU}(\text{Dense}(\text{LayerNorm}(x))) \in \mathbb{R}^{2h} \quad (46)$$

$$y = \text{Dropout}_{0.18}(\text{Dense}(\text{LayerNorm}(\bar{x}))) \in \mathbb{R}^{32} \quad (47)$$

Secondly, a function $\text{Embed}_d(j) \in \mathbb{R}^d$ which selects the j^{th} row from an implicit learnable weight matrix.

Chemical Features The chemical features used in this work are shown in Table A.1. To embed the categorical

Table A.1. Chemical input feature selection for PCQM4Mv2.

Node features	Feature Set			
	Original	Set 1	Set 2	Set 3
Atomic number	✓	✓	✓	✓
Group	.	✓	✓	✓
Period	.	✓	✓	✓
Element type	.	✓	✓	✓
Chiral tag	✓	.	.	.
Degree	✓	✓	✓	✓
Formal charge	✓	✓	.	✓
# Hydrogens	✓	✓	✓	✓
# Radical electrons	✓	✓	✓	✓
Hybridisation	✓	.	✓	✓
Is aromatic	✓	✓	✓	.
Is in ring	✓	✓	✓	✓
Is chiral center	.	✓	✓	✓

Edge features
Bond type
Bond stereo
Is conjugated
Is in ring

chemical features from the dataset $\mathbf{x}_i, \mathbf{e}_{uv}$ into a continuous vector space, we learn a simple embedding vector for each category, sum the embeddings for all categories, and then process it with an MLP to produce \mathbf{X}^{atom} and \mathbf{E}^{bond} , i.e.

$$\forall i : \bar{\mathbf{x}}_i^{\text{atom}} = \text{MLP}_{\text{node}} \left(\sum_{j \in \mathbf{x}_i} \text{Embed}_{64}(j) \right) \quad (47)$$

$$\forall i : \mathbf{x}_i^{\text{atom}} = \text{Dropout}_{0.18}(\bar{\mathbf{x}}_i^{\text{atom}}) \in \mathbb{R}^{d_{\text{node}}} \quad (48)$$

$$\forall (u, v) : \bar{\mathbf{e}}_{uv}^{\text{bond}} = \text{MLP}_{\text{edge}} \left(\sum_{j \in \mathbf{e}_{uv}} \text{Embed}_{64}(j) \right) \quad (49)$$

$$\forall (u, v) : \mathbf{e}_{uv}^{\text{bond}} = \text{Dropout}_{0.18}(\bar{\mathbf{e}}_{uv}^{\text{bond}}) \in \mathbb{R}^{d_{\text{edge}}} \quad (50)$$

Here MLP_{node} and MLP_{edge} refer to the functions by the same names used in Eq. 23 and 25 in the MPNN module, yet parameterised independently.

Graph Laplacian Positional Encodings (Kreuzer et al., 2021; Dwivedi & Bresson, 2020) Given a graph with adjacency matrix \mathbf{A} and degree matrix \mathbf{D} , the eigendecomposition of the graph Laplacian \mathbf{L} is formulated into a global positional encoding as follows.

$$\forall i : \mathbf{x}_i^{\text{LapVec}} = \text{MLP}_{\text{encoder}}(\mathbf{U} [i, 2 \dots k^{\text{Lap}}]) \in \mathbb{R}^{32}, \quad \text{where } \mathbf{L} = \mathbf{D} - \mathbf{A} = \mathbf{U}^{\top} \mathbf{\Lambda} \mathbf{U} \quad (51)$$

$$\forall i : \mathbf{x}_i^{\text{LapVal}} = \text{MLP}_{\text{encoder}} \left(\frac{\mathbf{\Lambda}'}{\|\mathbf{\Lambda}'\|} \right) \in \mathbb{R}^{32}, \quad \text{where } \mathbf{\Lambda}' = \text{diag}(\mathbf{\Lambda}) [2 \dots k^{\text{Lap}}] \quad (52)$$

To produce fixed shape inputs despite variable numbers of eigenvalues / eigenvectors per graph, we truncate / pad to the lowest 7 eigenvalues, excluding the first trivial eigenvalue $\Lambda_{11} = 0$. We also randomise the eigenvector sign every epoch which is otherwise arbitrarily defined.

Random Walk Structural Encoding (Dwivedi et al., 2022) This feature captures the probability that a random graph walk starting at node i will finish back at node i , and is computed using powers of the transition matrix \mathbf{P} . This feature captures information about the local structures in the neighbourhood around each node, with the degree of locality controlled by the number of steps. For this submission random walks from 1 up to $k^{\text{RW}} = 16$ steps were computed to form the feature vector.

$$\forall i : \bar{\mathbf{x}}_i^{\text{RW}} = \left[(\mathbf{P}^1)_{ii}, (\mathbf{P}^2)_{ii}, \dots, (\mathbf{P}^{k^{\text{RW}}})_{ii} \right] \text{ where } \mathbf{P} = \mathbf{D}^{-1} \mathbf{A} \quad (53)$$

$$\forall i : \mathbf{x}_i^{\text{RW}} = \text{MLP}_{\text{encoder}}(\bar{\mathbf{x}}_i^{\text{RW}}) \in \mathbb{R}^{32}, \quad (54)$$

Local Graph Centrality Encoding (Ying et al., 2021a; Shi et al., 2022) The graph centrality encoding is intended to allow the network to gauge the importance of a node based on its connectivity, by embedding the degree (number of incident edges) of each node into a learnable feature vector.

$$\forall i : \mathbf{x}_i^{\text{Cent}} = \text{Embed}_{64}(D_{ii}) \in \mathbb{R}^{64} \quad (55)$$

Shortest Path Distance Attention Bias Graphormer (Ying et al., 2021a; Shi et al., 2022) showed that graph topology information can be incorporated into a node transformer by adding learnable biases to the self-attention matrix depending on the distance between node pairs. During data preprocessing the SPD map $\Delta \in \mathbb{N}^{N \times N}$ is computed where Δ_{ij} is the number of edges in the shortest continuous path from node i to node j . During training each integer distance is embedded as a scalar attention bias term to create the SPD attention bias map $\mathbf{B}^{\text{SPD}} \in \mathbb{R}^{N \times N}$.

$$\forall i, j : B_{ij}^{\text{SPD}} = \text{Embed}_1(\Delta_{ij}) \in \mathbb{R} \quad (56)$$

Single-headed attention is assumed throughout this report for simplified notation, however, upon extension to multi-headed attention, one bias is learned per distance per head.

Embedding 3D Distances Using the 3D positional information provided by the dataset comes with a number of inherent difficulties. Firstly, the task is invariant to molecular rotations and translations, however, the 3D positions themselves are not. Secondly, the 3D conformer positions are only provided for the training data, not the validation or test data. To deal with these two issues and take advantage of the 3D positions provided we follow the approach of Luo et al. (2022).

To ensure rotational and translational invariance we use only the distances between atoms, not the positions directly. To embed the scalar distances into vector space \mathbb{R}^K we first apply $K = 128$ Gaussian kernel functions, where the k^{th} function is defined as

$$\forall i, j : \bar{\psi}_{ij}^k = \frac{\|\mathbf{r}_i - \mathbf{r}_j\| - \mu^k}{|\sigma^k|} \quad (57)$$

$$\forall i, j : \psi_{ij}^k = -\frac{1}{\sqrt{2\pi}|\sigma^k|} \exp\left(-\frac{1}{2}(\bar{\psi}_{ij}^k)^2\right) \in \mathbb{R} \quad (58)$$

with learnable parameters μ^k and σ^k . The K elements are concatenated into vector ψ_{ij} . We then process these distance embeddings in three ways to produce attention biases, node features and edge features.

3D Distance Attention Bias The 3D attention bias map $\mathbf{B}^{\text{3D}} \in \mathbb{R}^{N \times N}$ allows the model to modulate the information flowing between two node representations during self-attention based on the spatial distance between them, and are calculated as per (Luo et al., 2022)

$$\forall i, j : \mathbf{B}_{ij}^{\text{3D}} = \text{MLP}_{\text{bias3D}}(\psi_{ij}) \in \mathbb{R} \quad (59)$$

Upon extension to multi-headed attention with 32 heads $\text{MLP}_{\text{bias3D}}$ instead projects to \mathbb{R}^{32} .

Bond Length Encoding Whilst \mathbf{B}^{3D} makes inter-node distance information available to the self-attention module in a dense all-to-all manner as a matrix of simple scalar biases, we also make this information available to the MPNN module in a sparse but high-dimensional manner as edge features $\mathbf{E}^{\text{3D}} = [\mathbf{e}_{uv}^{\text{3D}} \text{ for } (u, v) \in \mathcal{E}]$ calculated as

$$\forall (u, v) : \mathbf{e}_{uv}^{\text{3D}} = \text{MLP}_{\text{encoder}}(\psi_{uv}) \in \mathbb{R}^{32} \quad (60)$$

Global 3D Centrality Encoding The 3D node centrality features $\mathbf{X}^{\text{3D}} = [\mathbf{x}_1^{\text{3D}}; \dots; \mathbf{x}_N^{\text{3D}}]$ are computed by summing the embedded 3D distances from node i to all other nodes. Since the sum commutes this feature cannot be used to determine the distance to a specific node, so serves as a centrality encoding rather than a positional encoding.

$$\forall i : \mathbf{x}_i^{\text{3D}} = W^{\text{3D}} \sum_{j \in \mathcal{V}} \psi_{ij} \in \mathbb{R}^{32} \quad (61)$$

Here $W^{\text{3D}} \in \mathbb{R}^{K \times 32}$ is a linear projection to the same latent size as the other encoded features.

B. Hardware and Acceleration

B.1. Hardware

We train our models using a BOW-POD16 which contains 16 IPU processors, delivering a total of 5.6 petaFLOPS of float16 compute and 14.4 GB of in-processor SRAM which is accessible at an aggregate bandwidth of over a petabyte per second. This compute and memory is then distributed evenly over 1472 tiles per chip. This architecture has two key attributes that enable high performance on GNN and other AI workloads (Bilbrey et al., 2022): memory is kept as close to the compute as possible (i.e., using on-chip SRAM rather than off-chip DRAM) which maximises bandwidth

Table A.2. Ensembled model performance on PCQM4Mv2 dataset. Models in the proxy set are trained on the `train+half_valid` data split whereas those in the full set are trained on all available data.

Case	Proxy Set		Main Set		Ensembling	
	# Models	Valid MAE		# Models		
		Avg.	Ensembled			
1: Baseline	10	0.0755	0.0725	35	1	
2: No Atomic Number	4	0.0761	0.0734	16	0.5	
3: FNN Dropout = 0.412	8	0.0759	0.0729	14	1	
4: FNN Dropout = 0.412; No Atomic Number	5	0.0761	0.0736	7	0.5	
5: Feature Set 2 [†]	4	0.0755	0.0731	15	1	
6: Feature Set 3 [†]	4	0.0754	0.0731	14	1	
7: Masking Weights = [1,2,2]	4	0.0754	0.0730	15	1	
All	39	0.0756	0.0722	112		

[†] As defined in Table A.1.

for a nominal power budget; and compute is split up into many small independent arithmetic units meaning that any available parallelism can be extremely well utilised. In particular this enables very high performance for sparse communication ops, like gather and scatter, and achieves high FLOP utilisation even with complex configurations of smaller matrix multiplications. Both of these cases are particularly prevalent in MPNN structures like those found in GPS++.

To exploit the architectural benefits of the IPU and maximise utilisation, understanding the program structure ahead of time is key. This means all programs must be compiled end-to-end, opening up a range of opportunities for optimisation but also adding the constraint that tensor shapes must be known and fixed at compile time.

B.2. Batching and Packing

To enable fixed tensor sizes with variable sized graphs it is common to *pad* the graphs to the max node and edge size in the dataset. This, however, can lead to lots of compute being wasted on padding operations, particularly in cases where there are large variations in the graph sizes. To combat this it is common to *pack* a number of graphs into a fixed size shape to minimise the amount of padding required, this is an abstraction that is common in graph software frameworks like PyTorch Geometric (Fey & Lenssen, 2019) and has been shown to achieve as much as 2x throughput improvement for variable length sequence models (Krell et al., 2021). Packing graphs into one single large pack, however, has a couple of significant downsides: the memory and compute complexity of all-to-all attention layers is $\mathcal{O}(n^2)$ in the pack size not the individual graph sizes, and allowing arbitrary communication between all nodes in the pack forces the compiler to choose sub-optimal parallelisation schemes for the gather/scatter operations.

To strike a balance between these two extremes we employ a two tiered hierarchical batching scheme that packs graphs

into a fixed size but then batches multiple packs to form the micro-batch. We define the maximum pack size to be 60 nodes, 120 edges and 8 graphs then use a simple streaming packing method where graphs are added to the pack until either the total nodes, edges or graphs exceeds the maximum size. This achieves 87% packing efficiency of the nodes and edges with on average 3.6 graphs per pack, though we believe that this could be increased by employing a more complex packing strategy (Krell et al., 2021). We then form micro-batches of 8 packs which are pipelined (Huang et al., 2018) over 4 IPUs accumulating over 8 micro-batches and replicated 4 times to form a global batch size of 921 graphs distributed over 16 IPUs.

B.3. Numerical Precision

To maximise compute throughput and maximise memory efficiency it is now common practice to use lower precision numerical formats in deep learning (Micikevicius et al., 2017). On IPUs using float16 increases the peak FLOP rate by 4x compared to float32 but also makes more effective usage of the high bandwidth on-chip SRAM. For this reason we use float16 for nearly all¹ compute but also use float16 for the majority² of the weights, this is made possible, without loss of accuracy, by enabling the hardware-level stochastic rounding of values. While we do use a loss scaling (Micikevicius et al., 2017) value of 1024 we find that our results are robust to a wide range of choices. We also use float16 for the first-order moment in Adam but keep the second-order moment in float32 due to the large dynamic range requirements of the sum-of-squares.

¹A few operations like the sum of squares the variance calculations are up-cast to float32 by the compiler.

²A small number of weights are kept in float32 for simplicity of the code rather than numerical stability.

C. Ensembling

C.1. Dataset Splits

While the original training set already contains 98% of the labelled data and all of the data with 3D positional information, we still aim to train on all available data for our final model. This, however, comes with many pitfalls due to inability to calculate a reliable measure of performance. Therefore, to understand the value of this additional data we consider an intermediate split configuration where we randomly sample half of the validation set (not resampled per run) to train on, holding the other half out for validation. As a result we have three dataset splits to consider: `original`, `train+valid` and `train+half_valid`.

C.2. Ensembling

Ensembling models has long been used to improve generalisation of machine learning models and has become an indispensable tool for practitioners entering machine learning competitions. Here we outline our ensembling strategy that aims to achieve confidence while training without a validation set, but also allows on-the-fly tuning and weighting of model ensembles. The main idea is to build two comparative model sets to ensemble, a *proxy* set and a *main* set. The proxy set is designed to be qualitatively similar to the main set but maintain a clean held out validation set by training on `train+half_valid`, whereas the main set is trained on `train+valid`. We aim for the proxy set to match the main set in all aspects apart from the training data and the number of models; to be able to focus computational resources on the main set we aim to build the proxy set to be approximately 25% of its size.

Diversity of models in an ensemble is a well known way to boost model performance (Zhou et al., 2002; Lakshminarayanan et al., 2017). In this work we propose six adjustments to the hyperparameters to form seven different model configurations to ensemble. In choosing these configurations we aim to build diversity in three main areas: input feature description (cases 2, 4, 5 and 6), regularisation strength (cases 2 and 3) and reliance on 3D features (case 7). As described in the previous paragraph we build a *proxy* set of models to help guide our ensembling strategy as well as a *main* set trained on all available data. The details of our seven configurations and their evaluation are shown in Table A.2.

Analysing the proxy set we found that reducing the weighting for the two worst performing models gave a small improvement to our final ensembled MAE, we therefore apply this is our main final ensemble too.

The final 112 model ensemble achieves an MAE of **71.9** meV on the test challenge set. This was completed in 1 hour 32 minutes using 1 IPU and AMD EPYC 7742 64-

Core CPU including all the feature processing, program compilation and model inference.